Towards Ultrathick Battery Electrodes: Aligned Carbon Nanotube–Enabled Architecture

*Kara Evanoff, Javed Khan, Alexander A. Balandin, Alexandre Magasinski, W. Jud Ready, Thomas F. Fuller, and Gleb Yushin**

Development of high-energy-density, long-lasting Li-ion batteries is desirable for portable applications, such as electronics and electric vehicles.[1] Both increasing the specific capacity of the battery electrodes and minimizing the relative weight and volume of inactive components (separators and metal foils)[2] by increasing the thickness of electrodes from the currently used 50–100 μm to hundreds of micrometers and above are attractive routes to achieve this goal.

Conventional electrodes contain active material mixed with conductive additives and a polymer binder. They commonly suffer from poor control over the resulting porosity, inhomogeneity,[3] tortuous electrolyte diffusion paths, and high electrical and, more importantly, high thermal resistance caused by point contacts between individual particles. These issues become particularly critical for nanopowder or thicker electrodes. Other challenges that need to be overcome for increasing the electrode thickness include formation of cracks within electrodes during the slurry drying process caused by the slow and uneven solvent evaporation throughout the thick layer, poor adhesion between the thick electrodes and metal current collectors, and the brittle behavior of thick electrodes. As a result, the overall progress on the development of thick electrodes has been very limited.[3]

Several interesting routes have been reported to decrease the electrode resistance by changing the current collector or electrode architecture. For example, the three-dimensional (3D) battery architecture[4] overcomes most of the limitations of the conventional technology, but its applications may likely be limited to microbatteries. Electrodeposited Cu or Al nanorods/nanowires have been successfully used as conductive supports for anodes[5] and cathodes.[4d] The use of vapor-deposited nanowires[6] have also shown potential for reduced electrode resistance and improved stability. However, the relatively high cost of these processes and slow nanowire growth rates impose some limitations on these technologies for thick electrode formation. Highly conductive vertically aligned carbon nanorods and C-Si nanotubes produced by pyrolysis of photoresist[7] and template-assisted vapor depositions,[8] respectively, have shown promising electrochemical behavior. However, the overall electrode thickness and the cost of the proposed process could similarly be a limiting factor for large size battery applications.

Here, we present an alternative scalable method to produce ultrathick, yet highly conductive and stable, Li-ion battery electrodes using vertically aligned carbon nanotubes (VACNTs) uniformly coated with a vapor-deposited active material layer. The recent developments in the rapid growth of VACNTs[9] allow low-cost formation of 1 mm or longer highly conductive tubes within minutes. The vapor deposition of anode (e.g., Si)[8] and cathode (e.g., LiV_2O_5)[10] materials may allow for the formation of uniform coatings on the CNT surface. The proposed architecture may offer unique benefits for the scalable formation of ultrathick electrodes, such as: 1) straight and aligned pores for rapid ion transport, 2) high thermal and electrical conductivity for high stability and long cycle life, 3) high structure uniformity combined with precise control over the dimensions of individual coated CNTs for predictable and reproducible performance, 4) a very smooth electrode surface which allows for thinner separators, 5) control over the electrode porosity achieved by electrode compression for the optimization of volumetric capacity and power characteristics, and 6) the absence of binder giving rise to improvements to the specific capacity and power performance.

For our proof-of-concept studies we selected a 1 mm thick VACNT electrode coated with Si and a thin C surface layer and demonstrated specific capacity in excess of 3000 $mAh \cdot g_{Si}^{-1}$ and cross-plane thermal conductivity in excess of 400 $W \cdot m^{-1} \cdot K^{-1}$. Our selection of Si was motivated by its high specific capacity and the tremendous interest in Si anode technology.[4b,6,8,11] The nano-dimensions of the Li–Si alloy coating minimize mechanical stresses.[12] In addition, the pores remaining within the VACNT electrode are needed for Si expansion during Li insertion. In contrast to a prior work on short VACNT-coated electrode,[13] we have demonstrated dramatically enhanced stability. To the best of our knowledge we report for the first time both the successful application of electrodes of large thickness for Li-ion batteries and the experimental demonstration of the

K. Evanoff, Dr. A. Magasinski, Prof. G. Yushin
School of Materials Science and Engineering
Georgia Institute of Technology
Atlanta, GA 30332, USA
E-mail: yushin@gatech.edu
J. Khan, Prof. A. A. Balandin
Department of Electrical Engineering
University of California
Riverside, CA, 92521, USA
K. Evanoff, Dr. W. J. Ready
Electro-Optical Systems Laboratory
Georgia Tech Research Institute
Atlanta, GA 30332, USA
Prof. T. F. Fuller
School of Chemical and Biomolecular Engineering
Georgia Institute of Technology
Atlanta, GA 30332, USA

DOI: 10.1002/adma.201103044

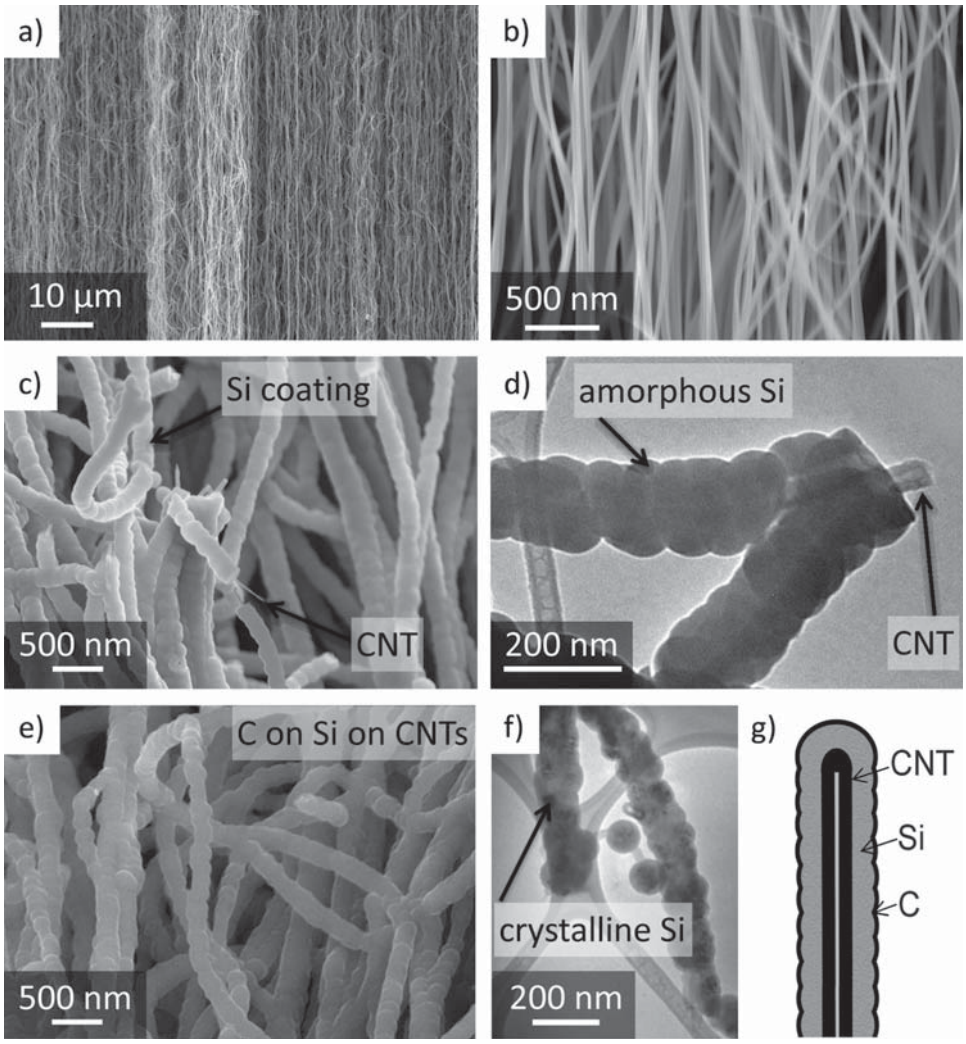

Figure 1. Cross-sectional SEM (a–c,e) and TEM (d,f) images of: synthesized VACNTs (a,b), Si coated VACNTs (c,d), and C and Si coated VACNTs (e,f). Schematic image of the final individual tube morphology (g).

VACNTs-enabled enhancements of their thermal and electrical conductivities by two-to-three orders of magnitude.

VACNTs were synthesized at 820 °C via a low pressure (~1000 Pa) chemical vapor deposition process (CVD) by using iron (II) chloride catalyst and acetylene gas precursor, as previously described.[9a] This method produces a high yield of VACNTs along the reaction chamber with measured growth rates in excess of ~0.1 mm·min^{-1}. In addition, this method does not require catalyst pre-deposition which reduces the process cost and sample preparation time. Scanning electron microscopy (SEM) images taken in cross-section show the high degree of alignment of the as-produced VACNTs at both low and high magnification (**Figure 1**a,b). A nano-Si coating was deposited onto VACNTs films by low pressure (500 °C, ~100 Pa) decomposition of SiH_4. Representative SEM and transmission electron microscopy (TEM) images show that the resulting Si forms rather uniform ~ 70 nm coating along the CNT length (Figure 1c,d). The deposited Si is amorphous, as indicated by the absence of crystallites in the TEM images (Figure 1d). Following, we utilized atmospheric pressure decomposition of C_3H_6 gas at 700 °C to deposit a thin C outer coating on the Si-coated VACNTs (Figure 1e) to improve the high rate performance, stability, and solid electrolyte interphase (SEI) layer. The importance of an outer C layer to achieve stable performance has been reported elsewhere.[11c–e] TEM images of the C and Si coated VACNTs show the formation of crystallites in the Si structure (Figure 1f). A schematic illustrating the final morphology and composition of individual nanotubes within the VACNTs film is shown in Figure 1g. The final Si:C composition and thickness ratios can be tailored by adjusting the reaction time for both deposition processes.

Raman spectroscopy (Figure S1, Supporting Information) and X-ray diffraction (XRD, Figure S2) studies followed the sample evolution. The Raman spectra of the as-produced VACNTs showed the characteristic G and D peaks with a low D band intensity thus indicating a small number of defects are present.[14] After Si deposition, a peak corresponding to Si emerged. After C coating, the Si band was still observable; however, the relative intensity in comparison with the D and G bands decreased thus confirming deposition (Figure S1).

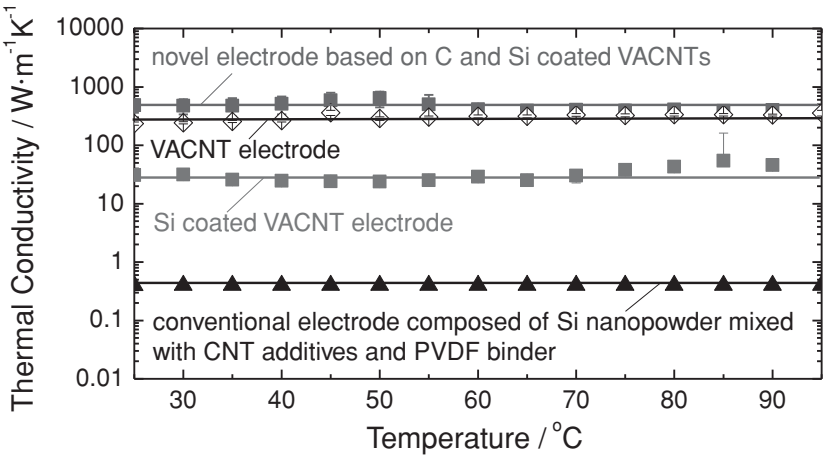

Figure 2. Comparison of the thermal conductivities of the conventional (bottom) and VACNTs-enabled (top) thick electrodes.

The XRD pattern of the as-produced VACNTs showed peaks corresponding to graphitic materials. After Si coating, the distinct graphitic peaks were no longer visible, rather broad peaks attributed to amorphous Si were observed (Figure S2) in agreement with the TEM observations (Figure 1d). Following C coating, the XRD pattern showed sharp peaks associated with crystalline Si and weaker peaks corresponding to C were visible (Figure S2).

High thermal and electrical conductivity of electrodes is desired for the majority of applications because most of the battery degradation mechanisms are thermally activated and related to processes on individual particles within electrodes, such as metal dissolution in cathodes or degradation of the SEI on the anodes.[15–17] Therefore, local heating caused by moderately high current pulses may severely diminish the battery cycle life, particularly if thick and more resistive electrodes are utilized.[15,17,18] Additionally, localized thermal and electrical gradients within electrodes give rise to highly undesirable unbalanced charging and discharging, which may lead to faster degradation and under-utilization of the available electrode capacity.[16,19] The importance of heat removal and thermal management of the batteries has been extensively discussed in recent literature.[16,19] Sophisticated methods of thermal management that employ microfluidic channels incorporated within the battery to transport cooling fluids were proposed to address this issue. These approaches, unfortunately, dramatically increase the cost and complexity of the battery production. Therefore, designing thick electrodes with very high thermal conductivity is of critical importance.

The thermal conductivities of VACNT–Si–C electrodes were measured using a noncontact optical laser flash technique. According to the established protocol, a xenon flash lamp produced shots with an energy of 10 $J \cdot pulse^{-1}$ on the sample surface while the temperature rise was measured at the other end with a nitrogen-cooled InSb infrared detector. The thermal-wave travel time allowed measurement of the thermal diffusivity α. The thermal conductivity K is related to α as $K = \alpha\rho C$, where ρ and C are the mass density and specific heat of the material, respectively. Details of the experimental setup and measurements procedures were reported elsewhere.[20] The system used for this study was calibrated with other techniques for measuring thermal conductivity such as transient planar source and 3-omega techniques.[20c,21] The K values measured for given samples are associated with the thermal conductivity along the VACNT–Si–C length and perpendicular to the electrode plane. Thermal conduction via CNT arrays dominates all other contributions to thermal transport owing to the extremely high intrinsic thermal conductivity of CNTs.[22] The heat losses via air are negligible for the transient method of measurements used in this work.

Figure 2 shows the results of the measurements for the coated VACNT-based electrodes compared with the conventional electrode of similar thickness composed of densely packed Si (<80 nm) and CNT powder (20 wt.% CNT) bonded with 10 wt.% polyvinylidene fluoride (PVDF). Although Si electrodes with porosity insufficient to accommodate Si expansion upon electrochemical alloying with Li show rapid degradation,[11e,11g] we wanted to compare the novel electrodes with that of a dense sample (which we will call "reference"), having the highest thermal conductivity achievable by using conventional electrode preparation methods. The effective thermal conductivity K determined for the CNT-containing reference powder electrode is ~0.4 $W \cdot m^{-1}K^{-1}$. In sharp contrast, the VACNT–Si–C electrode shows a three-order of magnitude improvement with K values in excess of 400 $W \cdot m^{-1} \cdot K^{-1}$. The increase in K translates to ~1000 times reduction of the thermal resistance t/K of the electrode (here t is the electrode thickness). The key reason for such a major improvement in the thermal properties of the electrodes is the extremely high intrinsic thermal conductivity of CNTs, which was reported to exceed 2000 $W \cdot m^{-1} \cdot K^{-1}$ and approach that of graphene.[23] The high degree of MWCNT alignment, their extension over the whole electrode thickness and the C shell coating the Si surface likely contribute to the very high thermal conductivity achieved. Our electrical measurements using a two-probe technique revealed ~100 times reduction of the electrical resistance of the VACNT-based electrode compared to our reference electrode (Figure S3).

Electrochemical measurements of the VACNT–Si–C electrode were performed in a 2016 coin cell configuration with a metallic Li foil counter electrode in the potential range of 0.01–1 V vs. Li/Li^+. Prior to cell assembly the active materials were adhered to a thin copper foil (**Figure 3**a) through thermal processes that created a conductive carbon interface with good adhesion. The VACNT–Si–C anode demonstrated very good stability for over 250 cycles (Figure 3b) and high specific capacity approaching theoretical limits (4200 $mAh \cdot g_{Si}^{-1}$), which indicates efficient electrical connectivity within the electrode and access of the electrolyte to all the deposited Si. The average values of dealloying capacities of the electrode at C/5 and C/2 were ~3300 $mAh \cdot g_{Si}^{-1}$ and ~2000 $mAh \cdot g_{Si}^{-1}$, respectively (Figure 3b).

We found that the outer C coating on the Si surface is critical to achieving good capacity retention and high Coulombic

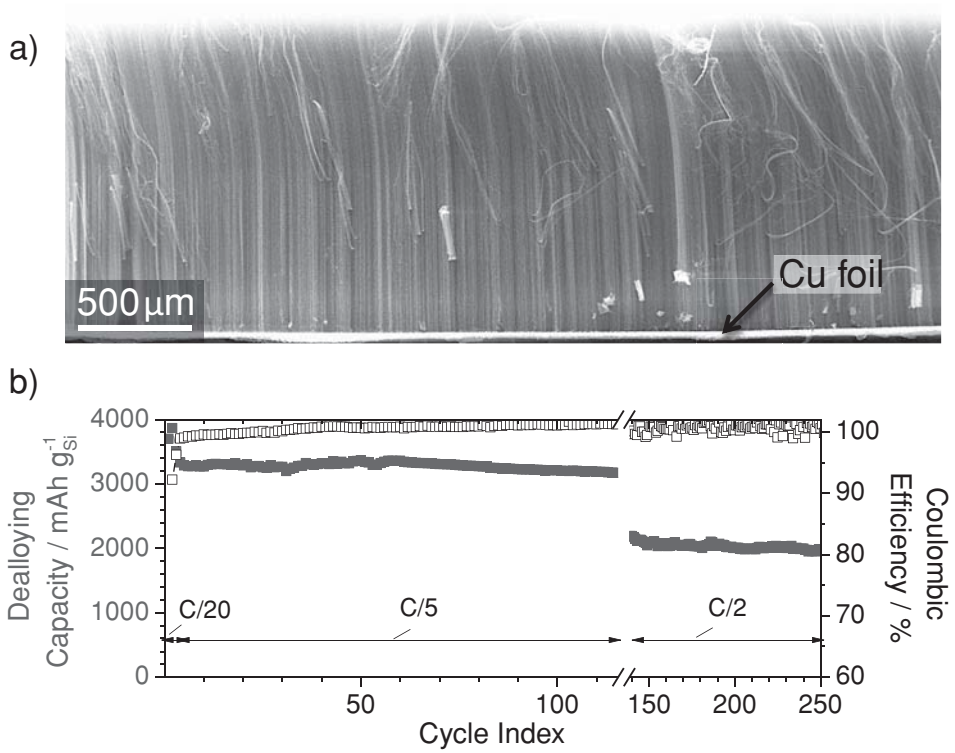

Figure 3. SEM image of a VACNT-based thick electrode adhered onto a thin copper foil (a). Dealloying capacity and Coulombic efficiency versus cycle number for the VACNT-Si-C electrode at three different current densities (b). The capacity is reported for the Si contribution only.

efficiencies (CE), confirming our prior studies.[8,11c–e] Without the C layer, Si-coated VACNT electrodes showed a noticeable decline in specific capacity at the rate of ~1% per cycle (Figure S4a). In addition, the unprotected Si showed relatively low values of CE < 98% (Figure S4b). In contrast, C-coated electrodes showed CE steadily increasing close to 100% (Figure S4b) and very stable performance with no signs of degradation (Figure S4a). The shape of the charge–discharge profiles (Figure S5a) and cyclic voltammograms (Figure S5b) of VACNT–Si–C electrode were very similar to our prior observations in various nanoSi-based anodes.[8,11c–e]

Although the observed rate capability of our 1 mm thick electrode was not very high, we expect that patterning of the electrode (for the formation of small interpenetrating channels for faster electrolyte access) as well as the modification of the electrolyte solvent may improve the high current/high power performance. In addition, we expect that substitution of Li foil with an actual cathode may further improve the rate capability.

In summary, we reported on the scalable formation of ultrathick electrodes that utilize VACNTs as a structured nanoscale platform with unique performance advantages. For example, the application of the VACNT architecture resulted in three and two orders of magnitude improvements in the electrodes' thermal and electrical conductivities, respectively. We have also shown that, when protected with a C layer, ultrathick Si-coated VACNTs electrodes can demonstrate stable performance at multiple current densities with reversible capacities significantly greater than graphite. Since the utilized structure allows for the stable performance of a commonly unstable material, we consider VACNTs as an attractive substrate for the deposition of other high capacity or low electrical or thermal conductivity materials to provide high energy and power characteristics, high electrical and thermal conductivities, and stable cycling for both cathodes and anodes.

Experimental Section

Si nanoparticles (98+%; US Research Nanomaterials, Inc., USA), CNTs (Arkema, USA) and PVDF (Sigma Aldrich, USA) were mixed by mortar and pestle and formed into a pellet using a pellet die (International Crystal Laboratories, USA) and hydraulic press (Carver Inc., USA) operating at ~8 Ton (applied pressure ~0.5 GPa). Each pellet contained Si:C:PVDF at the weight ratio of 7:2:1 with an average thickness of ~1 mm. Pellets of equivalent composition and thickness consisting of Si nanoparticles, Pure Black (Superior Graphite, USA), and PVDF were also formed using the previously described technique.

Microscopy images of the material morphology were captured by SEM (LEO 1530 and 1550, Germany; Hitachi S-4700, Japan) and TEM (JEOL 100 CX, Japan). SEM images were taken using several accelerating voltages (3–10 kV) and working distances (4–12 mm). An accelerating voltage of 100 kV was used for TEM imaging. For elemental and structural characterization Raman spectroscopy (WITec Instruments Corp., Germany) and XRD (PANalytical X'Pert PRO Alpha-1, USA) were utilized. Raman spectroscopy was performed using a 514 nm laser, 20× objective, and 600 grating with a 10 s integration time for 15 accumulations. XRD studies were conducted with a Cu Kα source with a monochromator using the following parameters: 45 kV accelerating voltage, 40 mA current, 0.033° 2θ step size, and 80–90 s record time. For diffraction analysis, Jade version 8 software (Materials Data, Inc., USA) with ICDD PDF-4 database was used.

The electrical measurements utilized a two probe technique in the cross-plane direction of the electrode (parallel to the VACNTs axis) using an Agilent B1500A analyzer. Tungsten metal probes with a tip radius of 0.5 μm were used. The electrical measurements were taken as a function of temperature by sweeping the voltage from –1 V to 1 V in 20 mV increments.

The ratio of Si to C for the electrodes was calculated from mass differences after each CVD reaction using a balance with 0.01 mg accuracy. Electrodes were spot-welded to 2016-type coin cells and degassed under vacuum at 70 °C overnight prior to assembly into half cells with a Li foil counter electrode (battery grade; Alfa Aesar, USA) in an Ar filled glovebox (<1 ppm H_2O, O_2). The electrolyte consisted of 1.0 M $LiPF_6$ in carbonates (Novolyte Technologies, USA). The cells were cycled between 10 mV and 2 V for VACNT–Si and 10 mV and 1 V for VACNT–Si–C on an Arbin BT2000 (Arbin Instruments, USA). The charge–discharge procedure utilized both constant current and constant voltage (at 10 mV to 20% of the initial current) regimes on the alloying step to ensure high degree of lithiation. The Coulombic efficiency was calculated as the percent ratio of the capacity after Li dealloying to after Li alloying. Cyclic voltammetry measurements were performed at a scan rate of 0.1 $mV \cdot s^{-1}$ using a multi-channel Solartron potentiostat (Solartron Analytical, USA).

Supporting Information

Supporting Information is available from the Wiley Online Library or from the author.

Acknowledgements

The authors acknowledge B. Hertzberg and J. Benson for construction of the CVD deposition systems and D. Teweldebrhan for assistance with the thermal conductivity measurement setup. The project was partially supported by Fred L. Hartley Family Foundation and NASA via Contract No. NNC08CB01C. K.E. was supported by the Robert Shackelford fellowship. The work at UCR was supported, in part, by the Winston Chung Global Energy Center.

Received: August 9, 2011
Revised: September 28, 2011
Published online: December 21, 2011

[1] A. S. Arico, P. Bruce, B. Scrosati, J.-M. Tarascon, W. van Schalkwijk, *Nat. Mater.* **2005**, *4*, 366.
[2] R. Moshtev, B. Johnson, *J. Power Sources* **2000**, *91*, 86.
[3] R. E. Garcia, Y.-M. Chiang, *J. Electrochem Soc.* **2007**, *154*, A856.
[4] a) J. W. Long, B. Dunn, D. R. Rolison, H. S. White, *Chem. Rev*. **2004**, *104*, 4463; b) T. Ripenbein, D. Golodnitsky, M. Nathan, E. Peled, *Electrochim. Acta* **2010**, *56*, 37; c) P. H. L. Notten, F. Roozeboom, R. A. H. Niessen, L. Baggetto, *Adv. Mater.* **2007**, *19*, 4564; d) M. M. Shaijumon, E. Perre, B. Daffos, P. L. Taberna, J. M. Tarascon, P. Simon, *Adv. Mater.* **2010**, *22*, 4978.
[5] a) L. Bazin, S. Mitra, P. L. Taberna, P. Poizot, M. Gressier, M. J. Menu, A. Barnabe, P. Simon, J. M. Tarascon, *J.Power Sources* **2009**, *188*, 578; b) P. L. Taberna, S. Mitra, P. Poizot, P. Simon, J. M. Tarascon, *Nat. Mater.* **2006**, *5*, 567.
[6] C. K. Chan, H. L. Peng, G. Liu, K. McIlwrath, X. F. Zhang, R. A. Huggins, Y. Cui, *Nat. Nanotech.* **2008**, *3*, 31.
[7] C. Wang, L. Taherabadi, G. Jia, M. Madou, Y. Yeh, B. Dunn, *Electrochem. Solid State Lett.* **2004**, *7*, A435.
[8] B. Hertzberg, A. Alexeev, G. Yushin, *J. Am. Chem. Soc.* **2010**, *132*, 8548.
[9] a) Y. Inoue, K. Kakihata, Y. Hirono, T. Horie, A. Ishida, H. Mimura, *Appl. Phys. Lett.* **2008**, *92*, 213113; b) V. N. Shanov, Y.-H. Yun, M. J. Schulz, *J. Univ. Chem. Technol. Met.* **2006**, *41*, 377.
[10] P. Liu, J. G. Zhang, J. A. Turner, C. E. Tracy, D. K. Benson, R. N. Bhattacharya, *Solid State Ionics* **1998**, *111*, 145.
[11] a) A. M. Wilson, B. M. Way, J. R. Dahn, T. Vanbuuren, *J. Appl. Phys.* **1995**, *77*, 2363; b) H. Kim, B. Han, J. Choo, J. Cho, *Angew. Chem. Int. Ed.* **2008**, *47*, 10151; c) K. Evanoff, A. Magasinski, J. Yang, Y. G., *Adv. Energy Mater.* **2011**, *1*, 495; d) A. Magasinski, P. Dixon, B. Hertzberg, A. Kvit, J. Ayala, G. Yushin, *Nat. Mater.* **2010**, *9*, 353; e) A. Magasinki, B. Zdyrko, I. Kovalenko, B. Hertzberg, I. Burtovyy, T. Fuller, I. Luzinov, G. Yushin, *ACS Appl. Mater. Interfaces* **2010**, *2*, 3004; f) Y. S. Hu, R. Demir-Cakan, M. M. Titirici, J. O. Muller, R. Schlogl, M. Antonietti, J. Maier, *Angew. Chem. Int. Ed.* **2008**, *47*, 1645; g) J. C. Guo, C. S. Wang, *Chem. Commun.* **2010**, *46*, 1428; h) J. S. Bridel, T. Azais, M. Morcrette, J. M. Tarascon, D. Larcher, *Chem.Mat.* **2010**, *22*, 1229; i) S. D. Beattie, D. Larcher, M. Morcrette, B. Simon, J. M. Tarascon, *J. Electrochem Soc.* **2008**, *155*, A158; j) I. Kovalenko, B. Zdyrko, A. Magasinski, B. Hertzberg, Z Milicev, R. Burtovyy, I Luzinov, G. Yushin, *Science* **2011**, 334, 75.
[12] a) R. A. Huggins, W. D. Nix, *Ionics* **2000**, *6*, 57; b) J. Graetz, C. C. Ahn, R. Yazami, B. Fultz, *Electrochem. Solid State Lett.* **2003**, *6*, A194.
[13] W. Wang, R. Epur, P. N. Kumta, *Electrochem. Commun.* **2011**, *13*, 429.
[14] a) E. F. Antunes, A. O. Lobo, E. J. Corat, V. J. Trava-Airoldi, A. A. Martin, C. Verissimo, *Carbon* **2006**, *44*, 2202; b) R. A. DiLeo, B. J. Landi, R. P. Raffaelle, *J. Appl. Phys.* **2007**, *101*, 064307.
[15] J. Vetter, P. Novak, M. R. Wagner, C. Veit, K. C. Moller, J. O. Besenhard, M. Winter, M. Wohlfahrt-Mehrens, C. Vogler, A. Hammouche, *J. Power Sources* **2005**, *147*, 269.
[16] T. M. Bandhauer, S. Garimella, T. F. Fuller, *J. Electrochem. Soc.* **2011**, *158*, R1.
[17] P. Ramadass, B. Haran, P. M. Gomadam, R. White, B. N. Popov, *J. Electrochem. Soc.* **2004**, *151*, A196.
[18] I. Bloom, B. W. Cole, J. J. Sohn, S. A. Jones, E. G. Polzin, V. S. Battaglia, G. L. Henriksen, C. Motloch, R. Richardson, T. Unkelhaeuser, D. Ingersoll, H. L. Case, *J. Power Sources* **2001**, *101*, 238.
[19] M. Fleckenstein, O. Bohlen, M. A. Roscher, B. Baker, *J. Power Sources* **2011**, *196*, 4769.
[20] a) S. Ghosh, D. Teweldebrhan, J. R. Morales, J. E. Garay, A. A. Balandin, *J. Appl. Phys.* **2009**, *106*, 113507; b) M. Shamsa, S. Ghosh, I. Calizo, V. Ralchenko, A. Popovich, A. A. Balandin, *J. Appl. Phys.* **2008**, *103*, 083538; c) R. Ikkawi, N. Amos, A. Lavrenov, A. Krichevsky, D. Teweldebrhan, S. Ghosh, A. A. Balandin, D. Litvinov, S. Khizroev, *J. Nanoelectron. Optoe.* **2008**, *3*, 44.
[21] M. Shamsa, W. Liu, A. A. Balandin, J. Liu, *Appl. Phys. Lett.* **2005**, *87*, 161921.
[22] A. A. Balandin, *Nat. Mater.* **2011**, *10*, 569.
[23] a) S. Ghosh, I. Calizo, D. Teweldebrhan, E. P. Pokatilov, D. L. Nika, A. A. Balandin, W. Bao, F. Miao, C. N. Lau, *Appl. Phys. Lett.* **2008**, *92*, 151911; b) A. A. Balandin, S. Ghosh, W. Z. Bao, I. Calizo, D. Teweldebrhan, F. Miao, C. N. Lau, *Nano Lett.* **2008**, *8*, 902.